Process monitoring of fibre reinforced composites using a multi-measurand fibre-optic sensor

Kochumulappon-Raghavan-Nair, Abilash-Kumar; Machavaram, Venkata R.; Mahendran, Ramani S.; Pandita, Surya D.; Paget, Christophe; Barrow, Colin; Fernando, Gerard F.

DOI:
10.1016/j.snb.2015.01.085

Sensors and Actuators B 212 (2015) 93–106

Contents lists available at ScienceDirect

Sensors and Actuators B: Chemical

journal homepage: www.elsevier.com/locate/snb

Process monitoring of fibre reinforced composites using a multi-measurand fibre-optic sensor

Abilash K. Nair[a], Venkata R. Machavaram[a,1], Ramani S. Mahendran[a], Surya D. Pandita[a], Christophe Paget[b], Colin Barrow[c], Gerard F. Fernando[a,*]

[a] School of Metallurgy and Materials, University of Birmingham, Birmingham, UK
[b] Airbus, Filton, UK
[c] Bruker UK Ltd, UK

ARTICLE INFO

Article history:
Received 7 October 2014
Received in revised form 10 January 2015
Accepted 20 January 2015
Available online 3 February 2015

Keywords:
Bragg grating
Extrinsic fibre Fabry–Perot interferometric sensor
Cure monitoring
Multi-measurand

ABSTRACT

This paper reports on the design, fabrication, characterisation and deployment of a multi-measurand optical fibre sensor (MMS) that is capable of simultaneously monitoring strain, temperature, refractive index and cross-linking chemistry. The sensor design is based on the extrinsic fibre Fabry–Perot interferometer. A feature of this sensor system is that a conventional multi-channel fibre-coupled near-infrared spectrometer is used to monitor the four independent parameters. The issues relating to the measurement resolution of the individual sensors and the associated interrogation equipment are discussed. The MMS was embedded in between the fourth and fifth plies of an eight-ply E-glass plain-weave fabric. A commercially available thermosetting epoxy/amine resin system was used to impregnate the fabric layers manually. The laminated preform was vacuum-bagged and cured in an autoclave. The following parameters were monitored: the depletion rates of the epoxy and amine functional groups in the resin system; the temperature in close proximity to the "chemical sensor"; the evolution of strain; and the refractive index of the resin system. The effect of post-processing on the output from the embedded optical fibre sensors is also considered.

1. Introduction

The production of composites using resin infusion of thermosetting matrices generally involves the following key steps: (i) impregnation of the reinforcement and/or the preform by the matrix; (ii) lay-up or lamination and consolidation of the impregnated perform; (iii) cross-linking of the matrix by the application of heat; and (iv) cooling the composite from the processing temperature to ambient.

The rate of chemical conversion of the functional groups present in the resin system can be influenced by parameters such as: (i) the stoichiometry of the resin and the hardener; (ii) the homogeneity of the mixed resin and the hardener; (iii) the volatility, chemical reactivity and integrity of the constituent components of the resin and hardener; (iv) the presence of contaminants, for example, moisture that can potentially react with the resin and/or hardener; (v) the rate of heating and the peak temperature experienced by the impregnated preform including the contribution from the exotherm; and (vi) the thermal management within the preform and the processing equipment during the cross-linking reactions.

Generalised representations of the cross-linking reactions for a typical epoxy/amine resin system are presented in Fig. 1. Reaction scheme-1 shows the initial reaction between the epoxy and amine functional groups; here the primary amine is converted to a secondary amine along with the formation of a hydroxyl functional group. The secondary amine (reaction scheme-2) is thus capable of reacting with a further epoxy functional group. Cross-linking reactions of this nature result in the conversion of the liquid or semi-solid monomer to a highly cross-linked and insoluble solid.

Side-reactions are also possible depending on the stoichiometry, processing temperature and the nature of contaminants present. Two such side-reactions are shown in Fig. 1 (reaction schemes-3 and 4). Reactions of this nature can add complexity to the analysis and interpretation of the cross-linking kinetics.

With reference to the design of the sensor systems to facilitate real-time process monitoring of composite preforms, reaction schemes-1 and 2 illustrated in Fig. 1 can be used to define the basic requirements.

* Corresponding author. Tel.: +44 1214148244.
E-mail address: g.fernando@bham.ac.uk (G.F. Fernando).
[1] Present address: School of Electronics Engineering, VIT University, Vellore 632014, Tamil Nadu, India.

http://dx.doi.org/10.1016/j.snb.2015.01.085

(i) Primary amine-epoxy addition

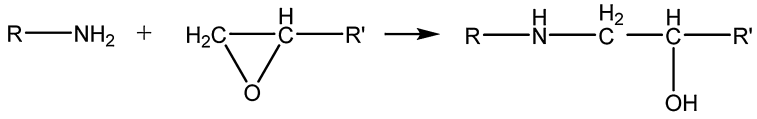

(1)

(ii) Secondary amine-epoxy addition

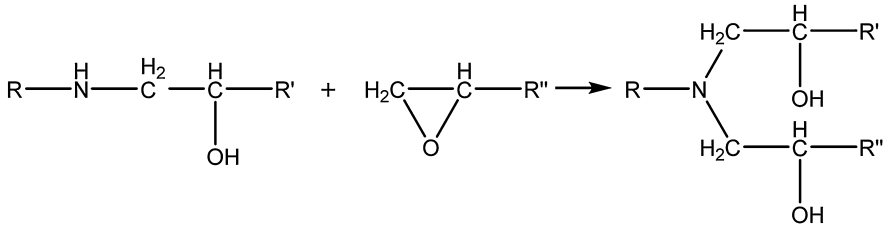

(2)

(iii) Etherification (epoxy/hydroxyl addition)

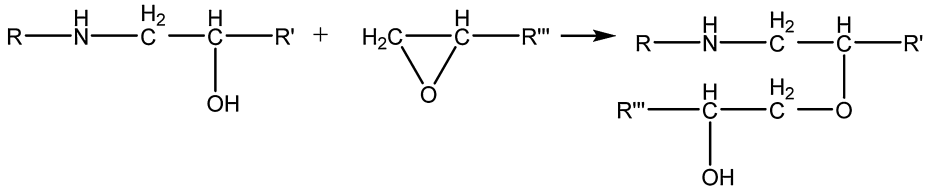

(3)

(iv) Epoxy homo-polymerisation

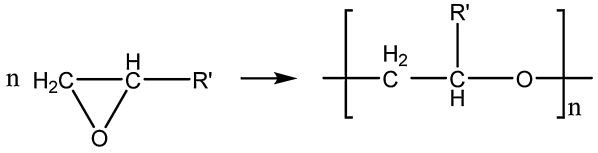

(4)

Fig. 1. Generalised reaction scheme for an epoxy/amine resin system [1].

(i) *Quantitative versus qualitative process monitoring*: Data on the quantitative depletion of the epoxy and amine functional groups can be obtained by transmission, reflection or evanescent wave near-infrared spectroscopy [1]. In these techniques, the absorbance bands associated with a non-reacting functional group (one that does not participate in the cross-linking reaction) is used to normalise the absorbance associated with the specific reactive functional groups. With reference to reaction schemes-1 and 2, the C–H absorbance band is generally used to normalise that associated with the epoxy, primary and secondary amine functional groups. This normalisation process is used to address path length changes during processing or when different sensors are used. The absorbance of the resin system in a conventional transmission infrared experiment can be described by the Beer–Lambert relationship:

$$A = \frac{\log_{10} I_0}{I} = \varepsilon c l \tag{5}$$

where

A = absorbance,
I_0 = intensity of the radiation entering the sample,
I = intensity of the radiation leaving the sample,
ε = extension coefficient or coefficient of absorption,
c = concentration of the absorbing species in the sample and
l = path length of the radiation within the sample.

Therefore, computing the area of the absorbance spectra for a specified functional group will enable its relative concentration to be established quantitatively.

From reaction schemes-1 and 2, the increase in the concentration of the OH functional group as a consequence of the cross-linking reaction can also be monitored to estimate the cross-linking kinetics [2].

Qualitative data on the rate of conversion of the reactive functional groups can be obtained by tracking the refractive index of the resin system [3]. As the molecular weight of the resin system increases as a function of cross-linking, the optical density increases in proportion. Hence, data on the progression of the cross-linking reactions or network formation can be inferred from the refractive index of the resin system. The refractive index is a function of temperature and the wavelength of light used in the measurement. Therefore, for refractive index-based process monitoring, it is necessary to monitor the temperature. Optical fibre-based sensor systems for monitoring the refractive index include core/cladding interactions where the matrix acts as cladding [4,5], reflections emanating from cleaved optical fibres immersed in the resin [3], cavities in optical fibres [6] and long-period gratings [7].

(ii) *Shrinkage*: Since the chemical reactions result in the formation of covalent bonds between the reacting functional groups, the resin system shrinks during chain extension and cross-linking [8]. Shrinkage of the matrix is a concern because it can lead to debonding between the reinforcement and the matrix. A number of techniques have been reviewed to quantify the magnitude of the shrinkage of thermosetting resins [9]. Optical fibre-based sensors have also been used to monitor the development of strain

in preforms during processing, including the following: (i) extrinsic fibre Fabry–Perot interferometric (EFPI) sensors [10]; (ii) fibre Bragg gratings (FBG) [11]; and (iii) Brillouin scattering [12].

(iii) *Temperature*: With reference to monitoring cross-linking kinetics, it is essential to monitor the heat transfer characteristics in and out of the preform. The ring-opening cross-linking reactions shown in Fig. 1 are exothermic and hence it is necessary to monitor and manage the thermal gradients within the preform during processing [2]. In general, laboratory-based processing equipment have a facility for heating and cooling to enable isothermal conditions to be maintained; this is necessary to obtain repeatable and reliable cross-linking kinetic data. However, if this is not the case, it will be necessary to monitor the temperature in close proximity to where the cross-linking data are acquired. Conventional thermocouples are used routinely along the perimeter of the preform. However, this assumes that the temperature at the perimeter is equivalent to that in the centre of the preform; this may not be so in the case of thick laminates. A number of researchers have demonstrated that EFPI [13] and FBG [14] sensors are suitable devices for monitoring temperature distributions in composites.

(iv) *Residual fabrication strain*: Since the reinforcing fibres and the matrix have different coefficients of thermal expansion, when the composite is cooled from the processing temperature, residual fabrication stresses can develop in the composite [15,16]. It is also known that other factors such as resin loss from the surface plies when bleeder-fabrics are used, and tool/preform interactions can contribute to the magnitude of the residual fabrication strains [17].

Considering the issues mentioned above, it is clear that a wide range of parameters can influence the cross-linking kinetics during processing. Therefore, the availability of a multi-measurand sensor system will enable cross-correlation to be established between the chemical reaction kinetics, processing schedules and the magnitude of residual fabrication stresses. A unique advantage of optical fibre sensor systems is that in addition to process monitoring, the same devices can be used for structural health monitoring [13]. However, the majority of the fibre optic-based sensor systems reported to-date for process monitoring (and structural health monitoring) have been single, or at the most, dual measurand systems [18]. A multi-parameter sensing concept for strain, temperature and vibration was reported by Rao et al. [19]. The feasibility of using an EFPI sensor design for monitoring strain in tandem with temperature logging via fluorescence-decay has also been demonstrated [20]. Singh et al. [21] reported the feasibility of multiplexing a number of EFPI sensors where the interrogation was carried out using a conventional Fourier transform infrared spectrometer.

Liu et al. [22] demonstrated an integrated EFPI/FBG sensor design for monitoring strain and temperature simultaneously. The interrogation was carried out using a low-resolution, low-cost CCD spectrometer. They used a spline-fitting routine to deconvolute the combined EFPI and FBG signals to overcome the ambiguity in determining the shift of the Bragg resonance and the interference fringes of the EFPI. The crosstalk was not found to be significant with the measurement technique that was used. Kang et al. [23] used a similar sensor design previously reported by Liu et al. [22] to monitor the strain and temperature of unsymmetrical composites. Ferreira et al. [24] decoupled the FBG signal from the combined EFPI and FBG signals by passing the signal through a Bragg grating that was similar to that used within the sensor-head. Machavaram et al. fabricated intrinsic Fabry–Perot cavities in optical fibres using an excimer laser [25], and hydrofluoric acid etching [26]. Rao et al. [27] also used laser ablation to create a cavity on the end-face of a fibre but in this instance, it was spliced to a long-period fibre grating for obtaining simultaneous information on the applied strain and temperature. An independent temperature calibration followed by straining sensor was used to demonstrate simultaneous monitoring of strain and temperature. Li et al. [28] reported on a hydrofluoric acid-etched intrinsic Fabry–Perot (FP) cavity in conjunction with an FBG to enable simultaneous monitoring of strain and temperature. The strain and temperature sensitivities of the Fabry–Perot cavity and the FBG were established independently. Jin et al. [29] used a pseudo-heterodyne ramp demodulation technique for deconvoluting the Fabry–Perot and FBG signals. The cross-talk between the signals was reduced to −40 dB.

The multi-measurand sensor reported in the current paper is based on the EFPI strain sensor design [30] but with the added functionality to monitor temperature, refractive index and the relative concentrations of specified functional groups. Unlike the previous EFPI/FBG sensor design [22], the current design negates the need for de-convoluting the EFPI/FBG signals. A feature of the multi-measurand sensor is that the interrogation of the four measurands is carried out using a multiport fibre-coupled Fourier transform near-infrared (FTNIR) spectrometer.

2. Experimental

2.1. Sensor design

A schematic illustration of the multi-measurand sensor (MMS) design is presented in Fig. 2 along with a description of the coded items.

i – cleaved single-mode optical fibre (SMF-28); i′ – photo-sensitive single-mode optical fibres (PS1250/1500); ii – precision-bore capillary tube; iii and iii′ – fusion joints; iv – fibre Bragg grating inscribed in close proximity to the cleaved photo-sensitive single-mode optical fibre; v – reflective coating on the single-mode photo-sensitive optical fibre; vi – air gap constituting the Fabry–Perot cavity; vii – reflective coating (Au/Pd) on the end-face of the capillary tube; viii – secondary multi-mode optical fibre secured on the SMF-28 optical fibre; ix – secondary cavities between the reflective end-face on the capillary and the cleaved end-faces of a pair of multi-mode optical fibres. These cavities serve as reservoirs for the resin system to enable transmission/reflection near-infrared spectroscopy; x – a pair of multi-mode optical fibres; xi – cleaved end-faces of a pair of multi-mode optical fibres serving as Fresnel reflection sensors to monitor the refractive index of the resin system; and xii – optional secondary optical fibre with a fibre Bragg grating that is secured on the single-mode SMF-28 optical fibres. Sections A, B, C, and D represent the EFPI/FBG, secondary cavity for transmission/reflection spectroscopy, optional secondary fibres for additional FBGs (not considered in the current study) and Fresnel reflection sensors to monitor the refractive index respectively.

2.2. Sensor manufacture

With reference to Fig. 2, Section [A] represents the combined EFPI/FBG strain/temperature sensor configuration where item [i] is a cleaved single-mode SMF-28 optical fibre (Corning Inc., USA). Item [i′] is a cleaved photo-sensitive single-mode optical fibre (PS1250/1500, Fibercore, UK), with an outer diameter of 125 ± 1 μm.

Component [ii] is a precision-bore capillary (Vitrocom, UK) with inner and outer diameters are 128 ± 3 and 300 ± 5 μm respectively. The capillary was supplied in a length of 1 m and the individual lengths of approximately 40 mm were cleaved using a capillary column cutter (Shortix™, SGT Singapore). The cleaved capillaries were immersed in an ultrasonic bath with isopropyl alcohol for 6 min and then dried at 100 °C for 15 min. The ends of the cleaved capillary were clamped on a fusion splicer (BFS 60, UK) and a sacrificial stripped and cleaned optical fibre was threaded into the capillary

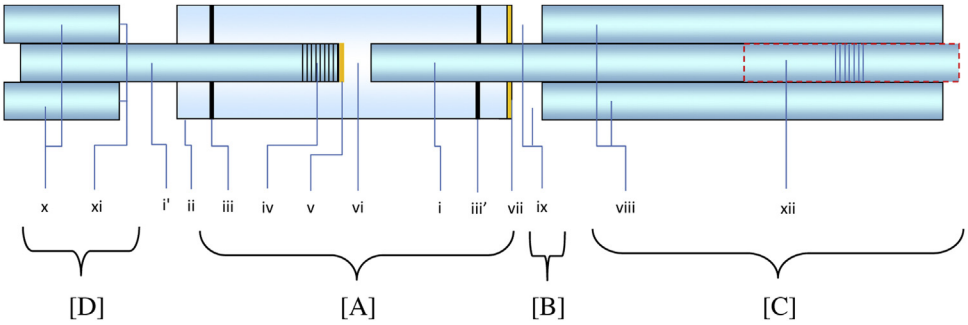

Fig. 2. Schematic illustration of the primary components of the multi-measurand fibre optic sensor. The coded items are described in the text.

to reduce the prospect of contaminating the bore of the capillary. The ends of the capillary were subjected a 20 mA arc-discharge for 1 s to remove any microscopic surface asperities. One face of the cleaved and arc-cleaned capillary end-face was sputter-coated (SC7640, Quorum Technologies, UK) with a gold–palladium (Au/Pd) alloy to create a reflective surface. The sputter-coating was carried out for 9 min using a plasma current of 20 mA and a vacuum of 10 Pa (0.1 mbar). The thickness of the coating was approximated using Eq. (6) [34]:

$$d = K^{*}I^{*}V^{*}t \tag{6}$$

where d is the coating thickness in Angstroms, K is 0.17 (an experimentally determined constant for a target-to-sample distance of 45 mm) for the Au/Pd target used in an argon environment, I is the plasma current in mA, V is the applied voltage in kV and t is the sputtering time in seconds. The thickness of the coating was calculated to be 183 nm.

A Bragg grating [iv] was inscribed on a stripped and cleaned portion of the photo-sensitive Ge–B co-doped optical fibre (PS1250/1500, Fibercore Ltd, UK) using a 1540 nm phase mask in conjunction with a krypton fluoride excimer laser (Braggstar, Coherent, UK) operating at 248 nm with a pulse energy of 10 mJ. The peak reflectivity of the Bragg grating was centred at 1539.84 nm. The reflectivity of the FBG was >90%. This fibre was cleaved in close proximity to the distal-end of the Bragg grating and the cleaved-end was sputter-coated [v] with Au/Pd as described previously.

The coated optical fibre with the Bragg grating and the capillary were annealed at 150 °C for 12 h in an air-circulating oven. This annealing schedule was derived from a series of experiments where the reflectivity and the dimensional stability of the gold coating were studied as a function of the annealing time and temperature.

The cleaved fibres (SMF-28) [i] and the gold-coated fibre (PS1250/1500) with the inscribed FBG [i′] were mounted on the fusion splicer and threaded carefully into the capillary [ii]. The gap between the cleaved end-faces [vi] was monitored using a FBG interrogation system (FiberPro IS7000). Once the desired cavity length was attained, the optical fibres were secured to the capillary via two fusion joints [iii and iii′] using an arc discharge current of 17 mA for 3 s; this process was repeated five times. The gauge length (distance between the fusion joints) was measured and the general profiles of the fusion joints were inspected using a binocular microscope (Leica Wild M3C).

In Fig. 2, Section [B] represents the secondary cavity that was created to enable transmission/reflection spectroscopy. The secondary cavity [ix] as illustrated in Fig. 2 was created by securing two cleaved multi-mode optical fibres [viii] (105/125 μm, Aomolin, China) on fibre [i]; the cavity length was 500 μm. The multi-mode optical fibres were surface-mounted to fibre [i] using a UV-curable adhesive (NOA 68, Norland Products Inc. USA). The cleaved-ends of the multi-mode fibres were aligned with the gold-coated end-face of the capillary using a 3D micro-translation stage (Newport, UK). This secondary cavity served as the reservoir for the resin thus permitting transmission/reflection spectroscopy to be conducted via the multi-mode optical fibres.

Section [C] in Fig. 2 illustrates options for mounting additional optical fibre sensors [xii]. For example, a fibre Bragg grating(s) or partially declad fibre to enable evanescent wave spectroscopy [31] or tapered sensor to monitor displacement [32].

With reference to Fig. 2, Section [D] illustrates the situation where two additional cleaved multi-mode optical fibres [x] were surface-bonded on fibre [i′] approximately 50 mm from the end-face of the capillary. This was done to prevent reflections from the end-face of the capillary coupling back into the fibres. These fibres served to monitor the Fresnel reflectivity [xi] at the cleaved end-faces. As mentioned previously, the Fresnel reflectivity is a function of the optical density of the resin system.

2.3. Annealing the gold/palladium coatings

With reference to the sensor design shown in Fig. 2, the effect of annealing the sputter-coated Au/Pd-coatings on the cleaved-end of the optical fibre with the FBG (housed within the EFPI sensor) was studied. This was carried out by monitoring the intensity of the reflected light from the coated fibre-end when light from an amplified spontaneous emission (ASE) source (LPB-1550-D, Lumen Photonics, UK) emitting over a spectral region of 1450–1600 nm, was coupled into the fibre. The reflected light intensity was measured using the InGaAs detector of a fibre-coupled FTNIR spectrometer (MATRIX^{TM}-F Duplex, Bruker, UK). The annealing of the coated optical fibre-end was carried out at 180 °C over a specified number of heating/cooling cycles. The Fabry–Perot interference fringes formed via the cavity between the coated and uncoated cleaved end-faces was also monitored using the FTNIR spectrometer.

2.4. Interrogation of the MMS sensor

A schematic illustration of the sensor interrogation scheme for the MMS is presented in Fig. 3. The FTNIR spectrometer was housed with six pairs of fibre-coupled input and output channels. The ASE light source was used to illuminate the primary Fabry–Perot cavity and the FBG sensor. This was necessary because the coupling of the light from the internal light source of the FTNIR spectrometer to the single-mode fibre was inadequate; the spectrometer was designed to operate with SMA-terminated multi-mode optical fibres. The reflected signals from the Fabry–Perot cavity and the FBG were measured at a resolution of 0.96 and 0.24 nm respectively over 16 scans using the detector on the FTIR spectrometer.

With reference to Fig. 3a, the secondary cavities (chemical sensors) and the Fresnel sensors were illuminated using the internal light source of the FTNIR spectrometer. The spectral range of the spectrometer was 910–2500 nm. The monitoring of the

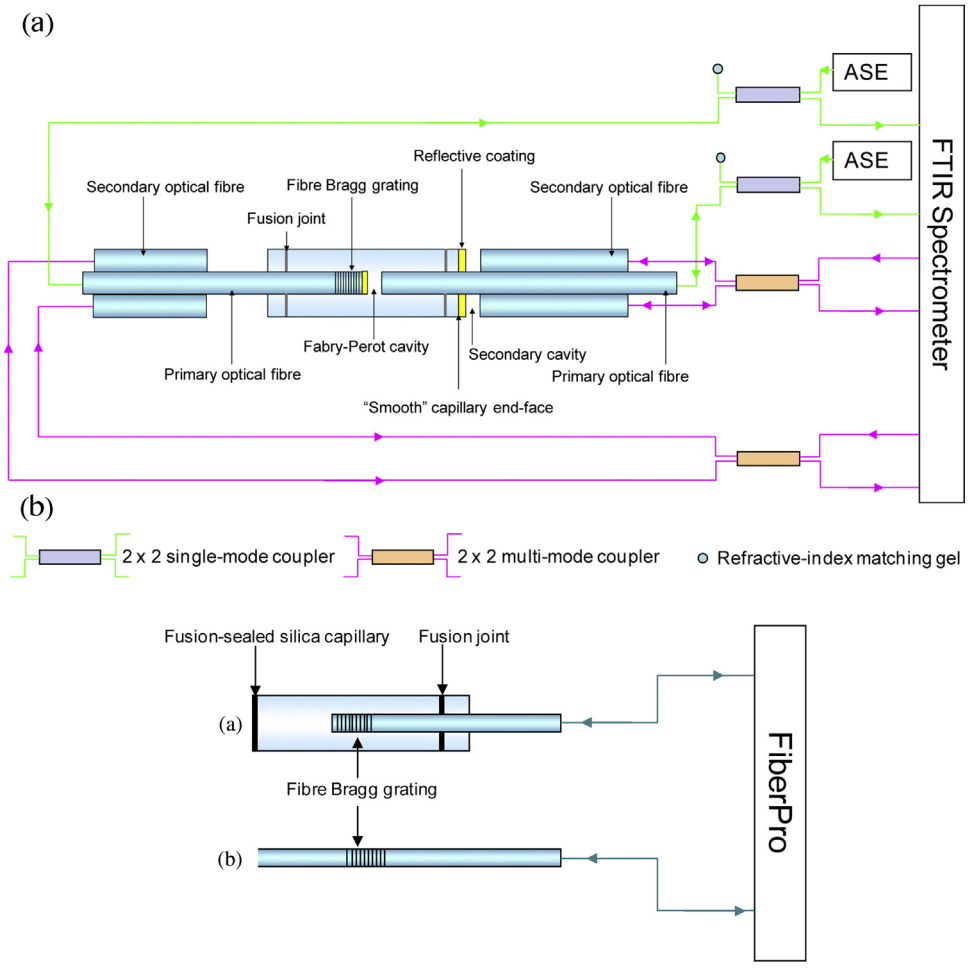

Fig. 3. (a) Schematic illustration of the experimental set-up for interrogating the multi-measurand sensor. (b) Schematic illustration of the independent FBG strain and temperature sensor interrogation set-up: (a) temperature sensor; and (b) strain and temperature sensor.

cross-linking reactions was performed at a resolution of 0.96 nm over 64 scans. In addition to the output from the multi-measurand sensor, the signals from the independent FBG-based temperature and strain sensors were acquired simultaneously using a multi-channel FBG interrogation unit (FiberPro IS7000). The wavelength accuracy and resolution of the FiberPro were ±0.005 nm and 0.001 nm respectively over a spectral range of 1530–1570 nm.

2.5. Autoclave-based process monitoring

A commercially-available thermosetting epoxy/amine resin system LY3505/XB3403 (Huntsman Advanced Materials, UK) was used to impregnate 8-plys of a plain-weave E-glass fabric. The E-glass fabric was donated by PD-Interglas Technologies, UK. The resin and the hardener were mixed in the ratio of 100:35 (by weight) respectively and the fabric layers were impregnated and laminated manually. The multi-measurand sensor was embedded in between the fourth and fifth plies of the eight-ply E-glass plain-weave fabric laminate. Polytetrafluoroethylene (PTFE) tubing was used to protect the optical fibres at the entry and exit points of the laminate. The ends of the PTFE tubes were sealed with the UV-curable epoxy resin to prevent the resin from wicking into the tube during processing. Conventional K-type wire thermocouples were also embedded in between plies 4 and 5 of the laminate at approximately 20–30 mm from the edge. A schematic illustration of the locations of the various sensors is shown in Fig. 4.

The laminated fabric with the embedded sensors was placed on a carbon fibre composite tool plate, vacuum-bagged using conventional procedures and processed in an autoclave (LBBC, UK). A schematic illustration of the various components of the vacuum bag assembly is shown in Fig. 5.

The vacuum bagged laminate was subjected to a vacuum of 0.1 MPa for 30 min prior to initiating the cross-linking cycle. The processing schedule used was as follows. The vacuum bagged assembly was heated from ambient to 120 °C at 2 °C per minute and the dwell time was 1 h. The pressure in the autoclave was increased from 0.007 MPa to 0.48 MPa at 0.02 MPa/min. The vacuum-bagged assembly was held at 120 °C for 1 h and then cooled to ambient temperature. The vacuum was maintained throughout the cure cycle and the autoclave pressure was maintained until the end of the isothermal dwell. The temperature on the surface of the vacuum bag was measured using an independent thermocouple. At the end of the cure cycle, the autoclave was turned off and allowed to cool naturally to ambient temperature.

3. Results and discussion

3.1. Quality of the cleaved capillary and the reflective coatings

Unlike the fabrication of conventional EFPI sensors [33], in the current case, it was necessary to pay special attention to the cleaved capillary as one end-face was destined to be used as a reflective

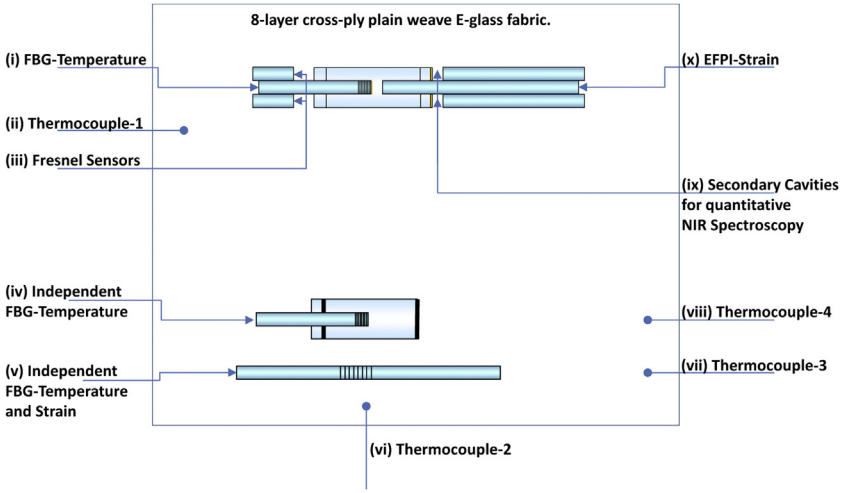

Fig. 4. Schematic illustration of the location of the MMS (EFPI, FBG-temperature, chemical and Fresnel reflection sensors) between the fourth and fifth plies of an eight-ply fabric laminate of dimensions 130 mm × 200 mm. The locations of the independent FBG-temperature, FBG-strain/temperature and conventional thermocouples are also indicated. The MMS was interrogated using a fibre-coupled FTNIR spectrometer. The two independent FBGs were interrogated using a 6-channel FBG interrogation unit.

surface for the chemical sensor. The processing routines used (ultrasonic and arc-cleaning) on the cleaved capillary were found to be satisfactory in obtaining repeatable quality and consistency with regard to the reflectivity of the end-face of the capillary.

The primary EFPI-FBG sensor with a cavity length of approximately 91 μm was fabricated prior to the construction of the secondary sensors (the chemical and Fresnel reflection sensors). The arc welded fusion joints were located approximately 10 mm from the Au/Pd coated end-face of the capillary. The fusion jointing processes did not degrade the reflectivity of the coating on the capillary.

3.2. Annealing the Au/Pd coatings

With reference to the EFPI/FBG sensor configuration illustrated in Fig. 2, the rationale for the reflective coating on the optical fibre with the FBG was to prevent cross-talk between the two sensor signals. However, this dictated the need to ensure that the presence of the reflective coating did not generate any unintentional influence or artefacts on the performance of the FBG and the EFPI sensors. Three issues were investigated: (i) the correlation between the reflectivity of the coating on the cleaved optical fibres and temperature cycling; (ii) the effect of the reflective coating on the response of the EFPI output; and (iii) the effect of temperature cycle on the output of the FBG.

The effect of temperature on the reflectivity of the coating on the cleaved-end of the optical fibre was investigated from ambient to 180 °C over four heat/cool cycles. The effect of this heating/cooling cycle on the reflectivity of the Au/Pd-coated fibres is shown in Fig. 6. The reflectivity measurements were carried out using the ASE light source and detector on the FTNIR spectrometer where the area under the reflected spectrum between 1450–1600 nm was calculated for specified temperature cycles. On inspecting Fig. 6, it can be seen that the reflectivity increased by approximately 1900% after the Au/Pd coating was applied.

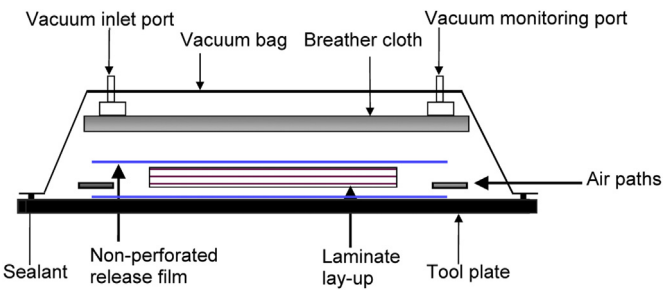

Fig. 5. Schematic illustration of the vacuum bagged assembly for the autoclave-based processing of the impregnated fabric laminate.

After the first heat/cool cycle, the average reflectivity of the coated fibres was increased by approximately 45% when compared to the reflectivity observed previously at 30 °C. A possible reason for the observed increase in the reflectivity is the consolidation and/or annealing of the Au/Pd particles in the sputter-coated film. Previous reports on annealing of thin gold films evince that irreversible morphological changes are mainly due to grain mobility and coalescence accompanied by improved adherence to glass substrates [40]. Subjecting the gold films to thermal cycles showed that the first thermal cycle produced permanent modifications to the microstructure. This was said to lead to improved structural stability with repeated thermal cycling [41]. The surface topography, band gap [42,43] and optical constants [44] of gold films on glass substrates were reported to be influenced strongly by the coating thickness and the annealing conditions.

From Fig. 6, the variation in the reflected intensities of the coated fibres after the second, third and fourth temperature cycles from 30 to 180 °C was less than 3%, indicating a stabilisation of the reflectivity of the coating.

Fig. 7 shows that the fringes of interference and the FBG signal are decoupled due to the design of the sensor (see Fig. 2). Hence, the coating and annealing conditions were concluded to be suitable for the production of the MMS sensor.

The effect of subjecting the Au/Pd coating to a series of heating and cooling cycles on the cavity length of the EFPI sensors was studied using two interrogation units (FiberPro and FTNIR spectrometer). A reference EFPI sensor (without the Au/Pd coating) and a coated EFPI sensor (with one of the fibres within the capillary being coated) with cavity lengths of 100 μm and 102 μm respectively were heated from 30 to 180 °C with 30 min dwells at 30, 90, 120, 150 and 180 °C. These experiments were carried out in an air-circulating oven and the cavity lengths were measured during the isothermal dwells. A K-type thermocouple was located in close proximity to the EFPI sensors to monitor the temperature. The sensors were interrogated using the FTNIR spectrometer and the FiberPro interrogation unit operating at wavelength resolutions of 0.96 nm and 1 pm respectively. The experiments were repeated

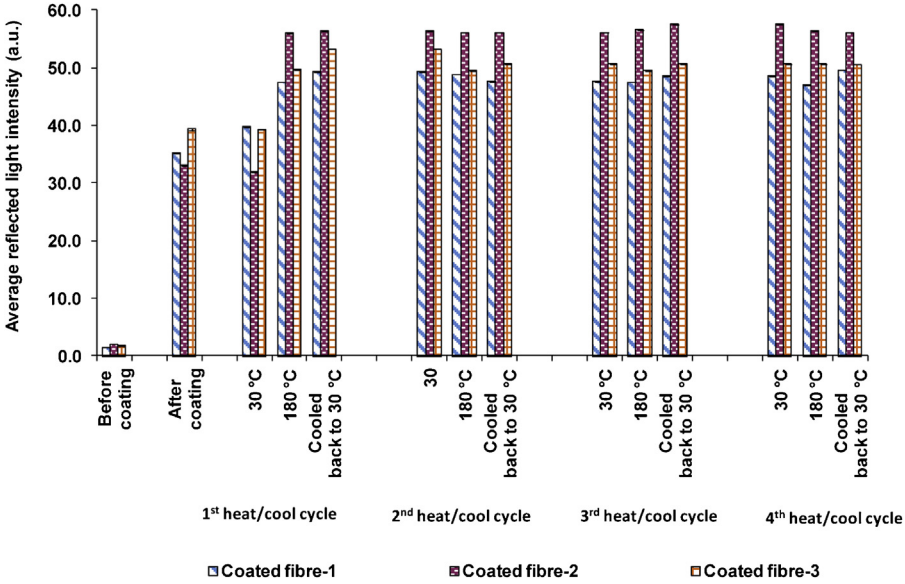

Fig. 6. Reflectivity of the gold/palladium coating on the cleaved end-faces of the optical fibres as a function of four heating/cooling cycles from 30 to 180 °C.

three times for each sensor using the two interrogation units. The absolute cavity length was calculated by determining the wavelengths corresponding to the adjacent maxima of the bright fringes [35].

In general, the temperature sensitivity of the EFPI sensor is relatively low due to: (i) the low thermal expansion of fused silica and the cleaved optical fibres in the capillary ($0.55 \times 10^{-6}\,°C^{-1}$); and (ii) the fact that the free-ends of the silica fibres and the capillary undergo thermal expansions in opposite directions. This cancels the effect of thermal expansion of the two components on the cavity length when the sensor is not embedded in the composite [36]. Given the higher resolution of the FiberPro interrogation unit, the thermally-induced changes in the cavity length of the EFPI can be measured more accurately. The data generated via the FiberPro interrogation unit and the FTNIR spectrometer are presented in Figs. 8 and 9 respectively where the insensitivity of the reference and coated-EFPI sensors when heated in air is apparent. The standard deviation for the cavity lengths for reference and coated EFPI sensors over the three heat/cool cycles was found to be less than 0.2 μm and 0.3 μm respectively. The percentage change in the cavity length at 30 °C for subsequent thermal cycle for the reference and coated EFPIs was less than 0.2% and 0.5% respectively. The cavity length of the reference and the reference EFPI sensor may show a small temperature sensitivity when they are heated in air due to one or more of the following reasons: (i) small difference in the thermal expansion of the fibre and fused silica capillary; (ii) distortion or deviation from geometrical symmetry in the fusion welds between the fibres and capillary and; (iii) the non-uniformity (physical and optical) of the sputter coating and the subsequent annealing and consolidation of the Au/Pd coating morphology.

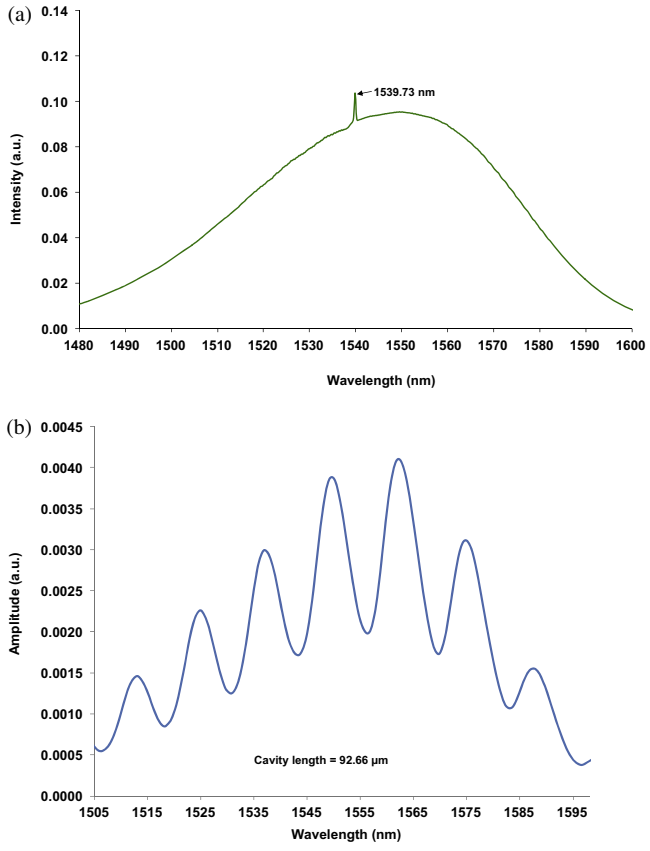

Fig. 7. Demonstration of the crosstalk-free FBG and EFPI spectra measured using the FTNIR spectrometer: (a) peak wavelength obtained from the FBG temperature sensor; and (b) interference fringes obtained from the EFPI sensor.

The effect of temperature cycling on the output of the FBG was also investigated. A reference FBG sensor (without the Au/Pd coating on the cleaved-end of the fibre) and a FBG sensor where the end of the cleaved optical fibre was coated, were heated from 30 to 180 °C with 30 min dwells at 30, 90, 120, 150 and 180 °C. The peak FBG reflected wavelengths for the reference and "coated" sensors were 1552.3 nm and 1552.5 nm respectively. These experiments were carried out in an air-circulating oven and the FBG peak shift was measured during the temperature dwells using the FTNIR spectrometer (0.24 nm resolution and 16 scans) and the FiberPro interrogation unit (1 pm resolution). A K-type thermocouple was located in close proximity to the FBG sensors to monitor the temperature.

The peak reflections for the reference and the coated FBGs measured using FiberPro showed negative shifts of 0.06 nm and 0.03 nm respectively after annealing and cooling to room temperature

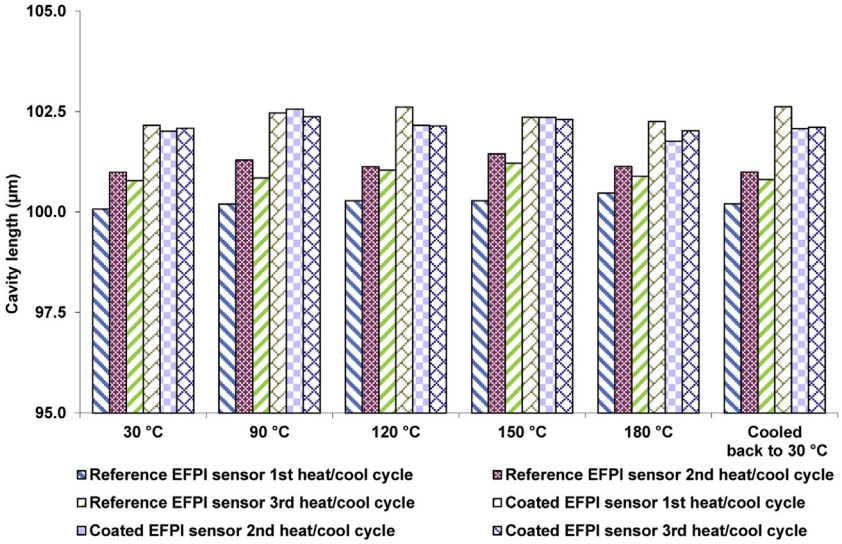

Fig. 8. Summary of the cavity lengths of the reference and Au/Pd coated EFPI sensors measured using the FiberPro interrogation unit over three heating/cooling cycles.

(30 °C). Thermal annealing of type-I Ge-B co-doped fibre gratings is said to lead to a negative shift in the Bragg wavelength accompanied by a drop in the reflectivity. This has been attributed to the decay of the grating structure [37,38]. The temperature sensitivities of FBGs at 1552.3 nm, determined using the FiberPro interrogation unit, during the 1st and 2nd heat/cool cycles for the reference and coated FBGs were in the range of 9.7–9.9 pm K^{-1} respectively by considering a linear fit. The data reported in the literature for the temperature sensitivity of type-I Ge–B co-doped optical fibre grating was in the range of 9.19–10.69 pm K^{-1} [45,46]. Accepting the lower wavelength resolution of the FTNIR spectrometer when compared with the FiberPro interrogation unit, the corresponding temperature sensitivities for the coated and reference FBG sensors measured via the FTNIR spectrometer were in the range of 9.5–10.2 pm K^{-1}.

With reference to the conclusions that were reached in the above-mentioned heating and cooling cycles for the reference and Au/PD coated devices, the annealing condition for the subsequent experiments were selected to be 150 °C for 12 h.

3.3. Process monitoring in the autoclave using the MMS

3.3.1. Data obtained from the electrical transducers in the autoclave

Fig. 10 shows the autoclave temperature via the in-built thermocouple, the temperature measured via the four thermocouples that were embedded in the E-glass preform and the pressure cycle as a function of the processing time. It is apparent that the temperature profiles obtained from the embedded thermocouples are similar. However, a thermal lag is observed between the embedded thermocouples and that recorded by the fixed thermocouple in the autoclave. The rate of heating experienced by the preform is approximately 1 K min^{-1} whereas that recorded by the autoclave is 2 K min^{-1}. The set isothermal temperature in the autoclave is attained after 54 min whereas the embedded thermocouples indicate that the desired temperature is achieved after 112 min. Moreover, the maximum temperature recorded by the embedded thermocouple is 121.8 °C; this most likely due to the exotherm as a consequence of the cross-linking reactions illustrated in Fig. 1.

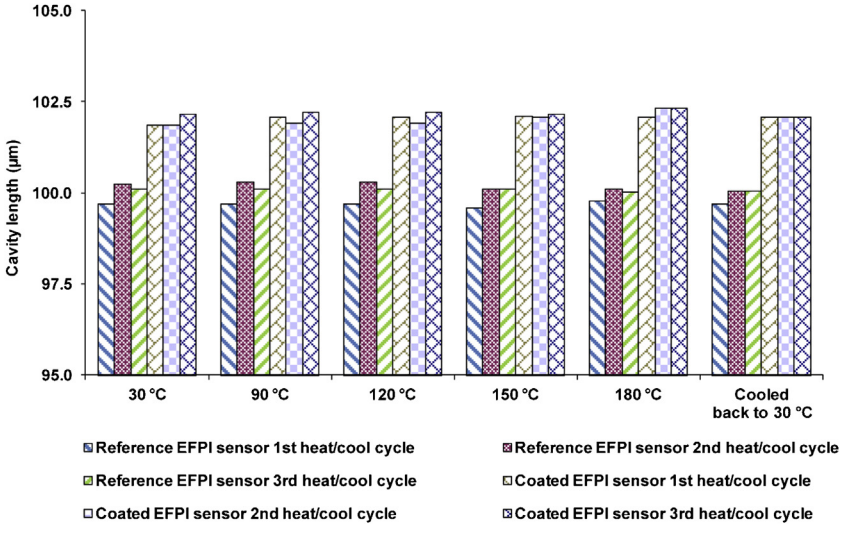

Fig. 9. Summary of the cavity lengths of the reference and Au/Pd coated EFPI sensors measured using FTNIR spectrometer over three heating/cooling cycles.

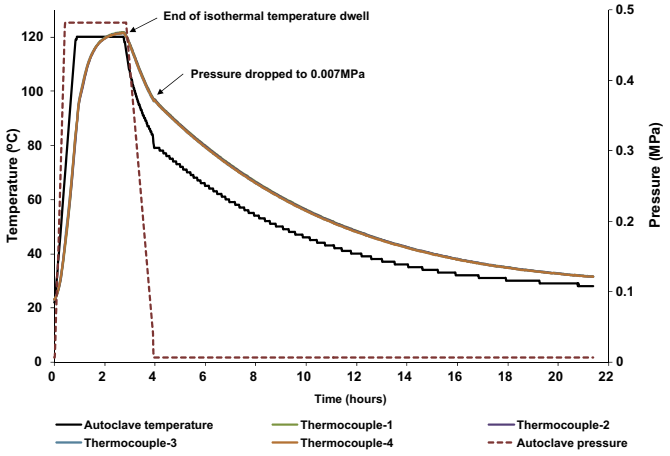

Fig. 10. Temperature and pressure profiles during the processing of the eight-ply E-glass fabric in the autoclave.

Inspecting the data from the embedded thermocouples, it is seen that the preform was above the desired isothermal temperature for approximately 60 min. After this period, the pressure was released to 0.007 MPa and the heating was terminated. The composite was then allowed to cool 30 °C prior to conducting a series of heating/cooling experiments.

3.3.2. Comparison of the FBG response and thermocouple data

The responses of the FBG-based temperature sensor that was housed within the capillary of the MMS, the independent FBG temperature sensor and one of the K-type thermocouple are presented in Fig. 11. Good correlation is observed between the three independent devices for monitoring the temperature. The consequence of the lower wavelength resolution of the FTNIR spectrometer is readily apparent in Fig. 11 during the cooling phase. Nevertheless, this limitation can be overcome using a spectrometer with a higher wavelength resolution.

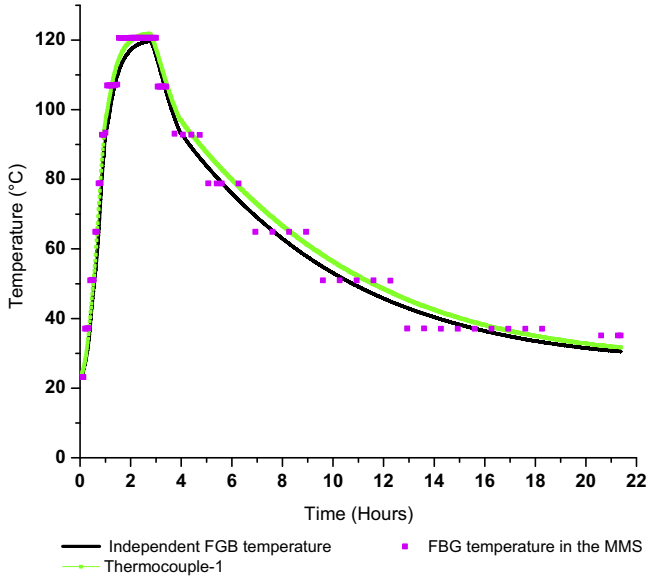

Fig. 11. Response of the FBG temperature sensor within the MMS, the independent FBG temperature sensor and an embedded thermocouple.

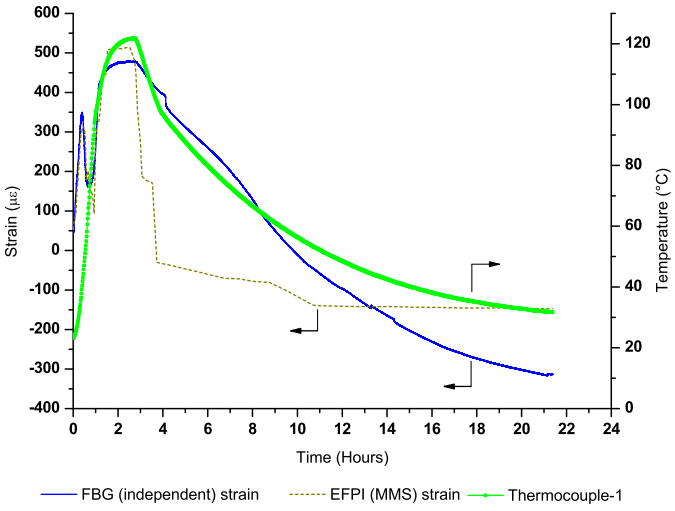

Fig. 12. The evolution of strain during the processing of the eight-ply woven E-glass fabric laminate. The strain data were measured using the EFPI (MMS) and the independent FBG sensors.

3.3.3. In situ strain monitoring in the preform during autoclave-based processing

The process-induced strains within the composite were measured using the primary cavity of the MMS and the independent FBG sensor (responsive to strain and temperature). With reference to the sensor design shown in Fig. 2, the interference signal of the primary cavity was decoupled from the Bragg reflection due to the reflective coating on the end of the fibre with the inscribed FBG. The absolute cavity length of the primary cavity was measured using the Fabry–Perot interference fringes obtained via the FTNIR spectrometer. The cavity length '*d*' as a function of the processing time was obtained using the following equation [35]:

$$d = \frac{\lambda_1 \lambda_2}{2 \cdot \Delta\lambda} \tag{7}$$

where λ_1 and λ_2 are the wavelengths corresponding to the maximum intensities of two adjacent bright fringes and $\Delta\lambda$ is the free spectral range of the EFPI. The longitudinal strain on the sensor can be expressed as the ratio of the change in cavity length to the gauge length (28.68 mm); with reference to Fig. 2, the gauge length is defined as the separation between the fusion joints in the MMS.

The influence of strain (ε) and temperature (T) on a fibre Bragg grating can be expressed as [39]:

$$\frac{\Delta\lambda_B}{\lambda_B} = (\alpha_{fibre} + \eta)\Delta T + (1 - p_e)\varepsilon \tag{8}$$

where λ_B (= $2\Lambda n_{eff}$) is the Bragg resonance wavelength; α_{fibre} is the coefficient of thermal expansion of the fibre; n_{eff} is the effective index of the core and Λ is the grating period; p_e is the photoelastic constant of the fibre; and η is the thermo-optic coefficient of the core. The response of the temperature sensing FBGs can be expressed as [39]:

$$\Delta T = \frac{\Delta\lambda_B}{\lambda_B(\alpha_{fibre} + \eta)} \tag{9}$$

The temperature sensitivity and the thermo-optic coefficient of annealed FBGs used in these experiments were 8.9 pm K^{-1} and 5.45×10^{-6} K^{-1} respectively. The thermal expansion coefficient and photoelastic coefficient of the fused silica fibre was assumed to be 0.55×10^{-6} K^{-1} and 0.22 respectively.

Fig. 12 shows the development of strain during processing of the E-glass preform in the autoclave. The evolution of the strain via the embedded MMS (EFPI sensor) during processing (cross-linking)

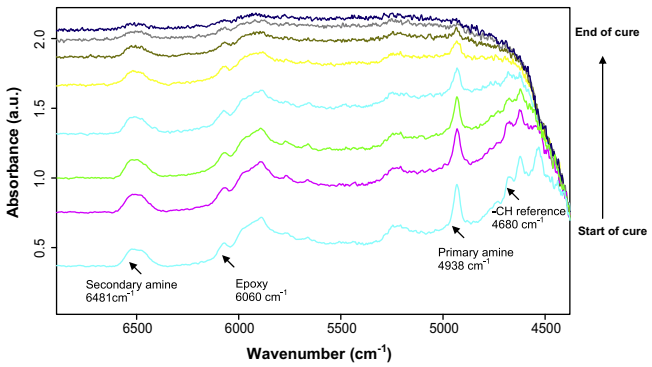

Fig. 13. Typical FTNIR spectra for the resin system obtained via the secondary cavities (chemical sensor) on the MMS during the cross-linking of the eight-ply woven E-glass fabric laminate at 120 °C.

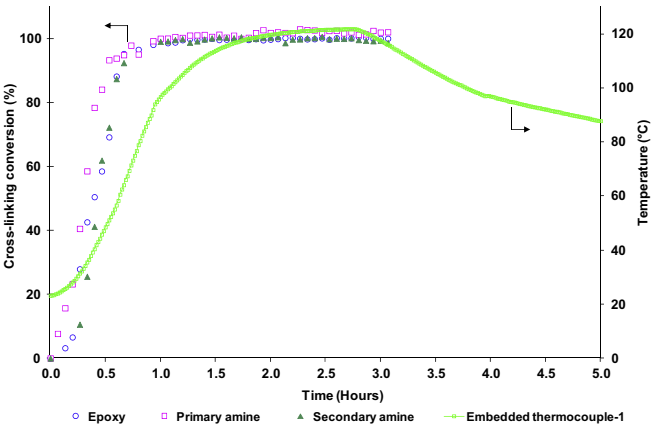

Fig. 14. The degree of conversion of the epoxy, primary amine and secondary amine functional groups via the multi-measurand chemical sensor. The cross-linking was carried out at 120 °C.

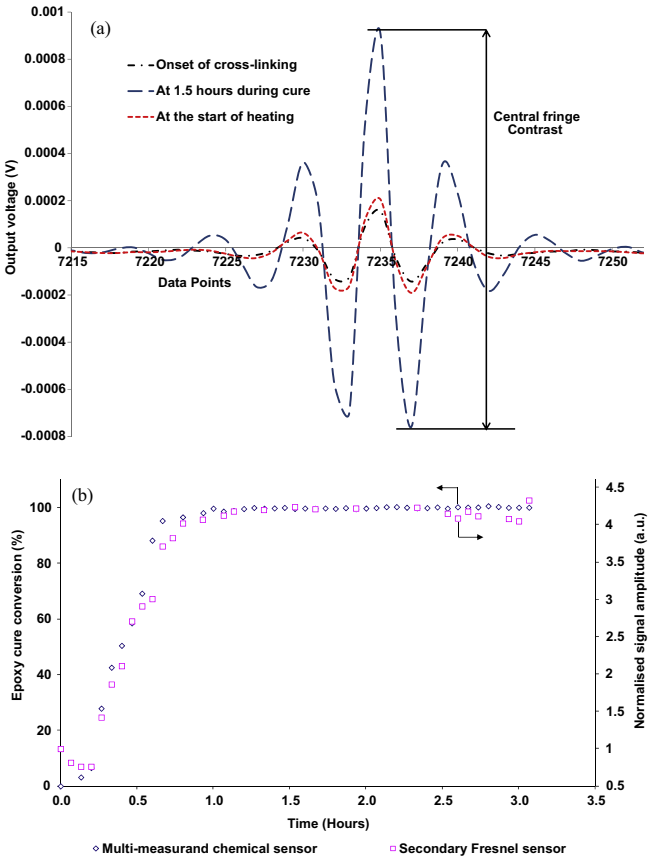

Fig. 15. (a) Examples of typical interferograms obtained from the FTNIR spectrometer in conjunction with the Fresnel sensor. (b) Correlation between the epoxy conversion presented previously in Fig. 14 and the amplitude of the interferogram measured using the FTNIR spectrometer via a secondary cleaved fibres (Fresnel reflection sensor).

was interrogated using the FTNIR spectrometer. The strain development in the preform was also measured using an independent FBG strain sensor via the FiberPro interrogation unit. The initial strain recorded by the sensors at the start of the processing cycle is attributed to the effect of de-bulking via the application of the vacuum.

In Fig. 12, as the temperature was increased from ambient, a tensile strain was recorded due to thermal expansion. However, at 45 °C, this trend reversed and a compressive strain was recorded, and this continued until 90 °C. Between 45 and 90 °C, the maximum/minimum strains recorded by the EFPI (MMS) and the independent FBG were 305.09/93.21 με and 345.67/167.96 με respectively. After 90 °C, the previously observed trend in the tensile strain resumed up to the dwell period.

The following factors may have been responsible for the observed trend in the strain profile. (i) The glass transition temperature (T_g) of the acrylate coating on the optical fibre: this was measured via a differential scanning calorimeter to be 78.6 °C (the heating rate was 20 K min^{-1}). Therefore, the loss of coupling efficiency between the optical fibre and the resin (matrix) may have occurred above the T_g of the acrylate coating. (ii) Deformation of the acrylate coating: it is possible that the acrylate coating may have deformed during the period when the pressure was applied and the subsequent relaxation above its T_g. The shrinkage of the resin during cross-linking is unlikely to be a primary factor because this behaviour was observed when the cured laminate was reheated and cooled three times (without pressure or vacuum in the autoclave). The sudden drop in the strain recorded by the EFPI sensor coincides with the period when the pressure in the autoclave was released.

The cross-linking data obtained from the chemical sensing device (secondary cavities) using the FTNIR spectrometer is presented in Fig. 14. It is seen that 95% conversion is attained after 40 min. Hence, it can be assumed that the stripped regions (capillary for the EFPI sensor and the stripped region where the FBG was inscribed) were bonded to the matrix. During the cooling phase, a reduction in the previously recorded strain was observed, as expected. The residual fabrication strain recorded at 30 °C measured using EFPI (MMS) and FBG (independent sensor) sensors were −147.49 and −313.98 με respectively. The strains measured at different stages of processing are summarised in Table 1.

3.3.4. *Monitoring the cross-linking reactions using the MMS chemical sensor*

Typical spectra obtained during the cross-linking of the LY3505/XB3403 resin system at 120 °C are shown in Fig. 13. The depletion of the amine and epoxy functional groups as a function of the processing time is readily apparent from the spectra. The epoxy peak at 6060 cm^{-1}, the primary amine peak at 4938 cm^{-1} and the secondary amine peak at 6481 cm^{-1} were selected for the quantitative analysis of the cross-linking process. The peak areas for the epoxy, primary and secondary amine absorbances were calculated by defining appropriate positions for the construction of the baseline. The C–H absorbance peak centred at 4680 cm^{-1} was used to normalise the areas of the epoxy, primary and secondary amine peaks.

Table 1
Summary of the strain at different stages of processing of the E-glass fabric laminate in the autoclave.

Sensor type	Before embedding (με)	After de-bulking (με)	At first observed drop in strain at 45 °C (με)	Min. at drop (με)	Max. at first recovery (με)	At the end of isothermal dwell at 120 °C (με)	Strain when pressure is released (με)	Residual strain at 30 °C (με)
EFPI (MMS) strain	0.00	53.36	305.09	93.21	508.25	478.02	−30.00	−147.49
Independent FBG strain	0.00	40.65	345.67	167.96	459.72	477.00	396.00	−313.98

Table 2
Summary of the strain measured in the cured fabric composite at different stages of post-processing: 1st; 2nd; and 3rd temperature cycles.

Temperature cycles	At the beginning of temperature cycle (με)	Max. before drop in strain (με)	Local min. before rise in strain (με)	At the end of isothermal dwell at 112 °C (με)	Residual strain at 30 °C (με)
1st post-cure temperature cycle					
EFPI (MMS) strain	−154.33	283.8	237.33	533.33	−145.60
Independent FBG strain	−123.30	271.61	246.72	468.24	−260.93
2nd post-cure temperature cycle					
EFPI (MMS) strain	−169.65	112.75	64.61	583.63	−143.85
Independent FBG strain	−117.65	292.7	255.5	479.71	−248.37
3rd post-cure temperature cycle					
Independent FBG strain	−188.40	281.98	263.93	478.95	−240.95

The depletion of the amine and epoxy functional groups as a function of processing time is readily apparent from the spectra shown in Fig. 13. The data for the degree of conversion shown in Fig. 14 was calculated from the spectra shown in Fig. 13 using the following equation [2]:

$$\alpha = 1 - \left(\frac{A_{EP,t}/A_{ref,t}}{A_{EP,0}/A_{ref,0}} \right) \quad (10)$$

where α is the conversion, $A_{ref,0}$ and $A_{ref,t}$ refer to the areas of the "inert" C–H reference peak at the start of the reaction ($t = 0$) and after time, t, respectively. $A_{EP,0}$ and $A_{EP,t}$ are the areas of the epoxy absorbance peaks for the uncured and partially cured resin at a specified time respectively. The relative rate of conversion of the primary amine is faster than that observed for the epoxy group; this may be attributed to the evaporation of the low molecular weight amine at the elevated processing temperature. The conclusion that can be reached is that the MMS was successful in tracking the depletion of the active functional groups in the resin system.

3.3.5. Refractive index monitoring via the Fresnel reflection sensor on the MMS

With reference to Fig. 15(a) and the interferograms obtained via the FTNIR spectrometer in conjunction with the Fresnel sensor, the contrast of the central fringe of the interferogram is taken as a measure of the Fresnel reflectivity at the cleaved fibre/resin interface; the contrast is determined by the intensities of the reference beam and the Fresnel reflection. The initial drop in the amplitude of the signal is due to a temperature-induced reduction in the density of the resin. As the temperature within the autoclave in increased, at some point, the cross-linking reactions become appreciable and this results in the optical density of the resin increasing. A detailed discussion on the output from multiple Fresnel sensors was reported by Machavaram et al. [47].

The fringe contrast shown in Fig. 15(b) is normalised with respect to that at the end of cure schedule. The refractive index of the resin system usually changes by an order of 10^{-2} as the resin is cured. The observed changes in the fringe contrast served as a qualitative means of cure progression as compared with the quantitative conversion data obtained via the secondary cavity. Fig. 15(b) shows the correlation between the degree of conversion of the epoxy/amine resin system shown previously in Fig. 14 and the amplitude of the interferogram obtained via the FTNIR spectrometer.

It can be concluded that the Fresnel reflection sensor on the MMS was capable of tracking the evolution of the refractive index of the resin system. Furthermore, good correlation is observed between the quantitative chemical sensor and qualitative Fresnel reflection sensor; both the sensors were interrogated using the FTNIR spectrometer.

3.4. Post-processing of the E-glass fabric composite

The cured fabric composite was subjected to three heating/cooling cycles in the autoclave and the strain was monitored simultaneously using the EFPI (MMS) and the independent FBG sensors. The maximum temperature recorded by the embedded thermocouple located in the mid-ply of the composite was 112 °C. The composite was kept at this temperature for 30 min without using the pressure and vacuum. After this period, the heating was terminated and the composite was allowed to cool to 30 °C. The measured strain in the composite using the EFPI (MMS) and the independent FBG sensors during the 1st and 2nd heating/cooling cycle is cross-plotted in Fig. 16(a) and (b). The strain recorded by the EFPI (MMS) and the independent FBG sensor at the start of the 1st and 2nd heating/cooling cycle were −154.33/−123.30 με and −169.65/−117.65 με respectively. As observed previously for the initial cross-linking cycle, a drop in the strain value is also observed between 58 and 73 °C. This may be attributed to the combined effects of the glass transition temperatures of the acrylate coating on the optical fibre and the resin system. The T_g of the acrylate coating and the resin system measured using a differential scanning calorimeter, at a heating rate of 20 K min^{-1}, were found to be 78.6 ± 0.9 °C and 79.6 ± 0.1 °C respectively. The laminate was subjected to a third heating/cooling cycle and the strain was monitored using the independent FBG sensor. The MMS was not interrogated in this instance because the data from the 1st and the 2nd heating/cooling cycles were similar. As shown in Fig. 16(c), the strain behaviour during the heating phase of the third temperature cycle was found to be similar to the first two cycles. The strain recorded by the independent FBG sensor at the start of the 3rd heating/cooling cycle was −188.40 με and the residual strain when the laminate was cooled to 30 °C was found to be −240.95 με.

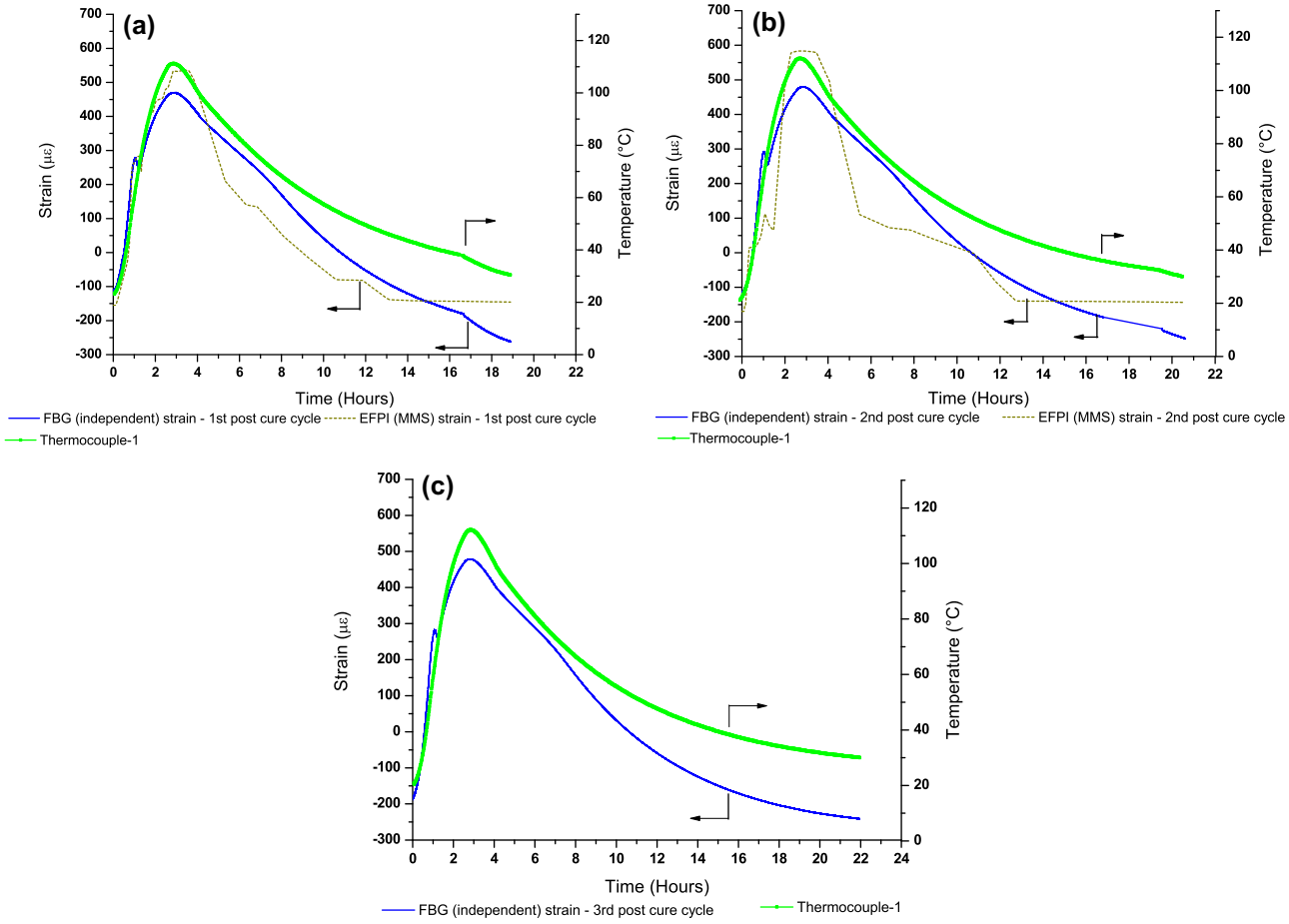

Fig. 16. (a) The strain recorded by the EFPI (MMS) and the independent FBG sensor during the first post cure temperature cycle of the eight-ply woven fabric preform. (b) The strain recorded by the EFPI (MMS) and the independent FBG sensor during the second post cure temperature cycle of the eight-ply woven fabric preform. (c) The strain recorded by the independent FBG sensor during the third post cure temperature cycle of the eight-ply woven fabric preform.

The strain values of the composite at different stages of the 1st, 2nd and 3rd temperature cycles are summarised in Table 2. It can be seen that the trend in the residual strain measured at 30 °C for the EFPI (MMS) and the FBG sensors is similar.

Linear regression lines were fitted to the FBG (independent) strain versus temperature data in Fig. 16(a)–(c) up to 54 °C during the heating phase; the thermal expansion of the composite was found to be $10.98 \times 10^{-6}\,K^{-1}$, $11.42 \times 10^{-6}\,K^{-1}$ and $12.30 \times 10^{-6}\,K^{-1}$ respectively. This may be indicative of post-curing in the composite as a function of the three heating/cooling cycles.

It is concluded that the data from the EFPI (MMS) and the independent sensors show a similar trend as far as the magnitude of the residual fabrication strain is concerned. However, further research is needed to explain the sudden drop in the EFPI data when the pressure in the autoclave is turned off. The discrepancy between the EFPI and FBG strain sensors may be due to the assumptions made in the decoupling of the strain from the temperature in the latter case. It is also known that the FBG is sensitive to off-axis strain.

4. Conclusions

A fibre-optic multi-measurand sensor based on the extrinsic fibre Fabry–Perot interferometer was designed to enable the monitoring of four independent parameters: the cross-linking kinetics; temperature; strain; and the evolution of the refractive index.

Good correlation was observed between the cross-linking data obtained using the MMS chemical sensor (secondary cavity) and independent cuvette-based transmission FTIR spectroscopy experiments.

Since the FBG that was housed within the EFPI sensor housing was sputter-coated with Au/Pd, annealing was necessary to stabilise the coating. It was found that a single annealing cycle (150 °C for 12 h) was sufficient to stabilise the coating over the temperature range investigated. The presence of the Au/Pd coating on the end-face of the fibre with the FBG was not seen to influence the output of the EFPI or FBG sensors.

An anomaly was observed in the output of the EFPI strain and independent FBG strain/temperature sensors. It is speculated that this anomaly may be due to a combination of the T_g of the resin system and that of the acrylate coating being exceeded. However, further work is needed to verify this hypothesis.

Good correlation was observed between the Fresnel sensor and the rate of conversion of the epoxy functional group. In other words, correlation was demonstrated between the quantitative spectral-based chemical and the qualitative refractive index sensors.

The MMS sensor was used to track the evolution of the residual fabrication stresses during autoclave-based processing. The feasibility of using the MMS to study the thermal expansion characteristics of the composites was demonstrated.

In conclusion, it is proposed that the MMS sensor can be used as an effective tool to study the chemical, thermal and physical ageing of polymers and fibre reinforced composites.

Acknowledgements

The authors wish to acknowledge financial support from the EPSRC (TS/G000387/1) and the Technology Strategy Board, Projects AB134K and BD072K. The support given by the industrial partners (CTM, Bruker UK, Mould Life, Pultrex, PPG, Luxfer Gas Cylinders, Halyard, and Huntsman Polyurethanes) is duly acknowledged. GF and VRM acknowledge the financial support provided by the Royal Society. AKN acknowledges the financial support given by Airbus, UK and Universities UK through an Overseas Research Scheme award. ANK acknowledges the assistance given by Drs L Wang, S Irfan and D Harris for specified aspects of the experimental work. The authors wish to acknowledge the technical assistance provided by BA Fernando, Professor Brian Ralph, Mark Paget and Frank Biddlestone.

References

[1] G.F. Fernando, B. Degamber, Int. Mater. Rev. 51 (2006) 65.
[2] R.S. Mahendran, L. Wang, V.R. Machavaram, R. Chen, S.N. Kukureka, G.F. Fernando, Opt. Laser Eng. 47 (2009) 1069.
[3] D. Harris, G.F. Fernando, Int. Conf. on Compos. Mater., ICCM-17, Edinburgh, UK July 27–31, Code 85394, 2009.
[4] K.Y. Lam, M.A. Afromowitz, Appl. Opt. 34 (1995) 5635.
[5] G.R. Powell, P.A. Crosby, G.F. Fernando, R.C. Spooncer, C.M. France, D.M. Waters, J. Smart Mater. Struct. 7 (1998) 557.
[6] V.R. Machavaram, R.A. Badcock, G.F. Fernando, J. Opt. A: Pure Appl. Opt. 14 (2012) 035602.
[7] J.P. Dunkers, J.L. Lenhart, S.R. Kueh, J.H. Van Zanten, S.G. Advani, R.S. Parnas, Opt. Laser Eng. 35 (2001) 91.
[8] G.F. Fernando, P.A. Crosby, T. Liu, in: K.T.V. Grattan, B.T. Meggitt (Eds.), Optical Fibre Sensor Technology, vol III, Kluwer Academic Publishers, 1999, ISBN 0412825708.
[9] D.U. Shah, P.J. Schubel, Polym. Test. 29 (6) (2010) 629.
[10] T. Liu, M. Wu, Y.J. Rao, D.A. Jackson, G.F. Fernando, Smart Mater. Struct. 7 (1998) 550.
[11] V. Dewynter-Marty, P. Ferdinand, E. Bocherens, R. Carbone, H. Beranger, S. Bourasseau, M. Dupont, D. Balageas, J. Intell. Mater. Syst. Struct. 9 (1998) 785.
[12] Y.A. Ito, S.B. Minakuchi, T.B. Mizutani, N.B. Takeda, Adv. Comp. Math. 21 (2012) 259.
[13] G.F. Fernando, T. Liu, P.A. Crosby, C. Doyle, A. Martin, D. Brooks, B. Ralph, R.A. Badcock, J. Meas. Sci. Technol. 8 (1997) 1065.
[14] M. LeBlanc, M. Huang, H. Shangyuan, R.M. Measures, Proc. SPIE 2444 (1995) 136.
[15] S.R. White, H.T. Hahn, J. Comp. Math. 26 (1992) 2402.
[16] T.A. Bogetti, J. Comp. Math. 26 (1992) 626.
[17] G. Fernlund, N. Rahman, R. Courdji, M. Bresslauer, A. Poursartip, K. Willden, K. Nelson, Comp. – Part A: Appl. Sci. Manuf. 33 (2002) 341.
[18] P.A. Crosby, C. Doyle, C.J. Tuck, M. Singh, G.F. Fernando, Proc. SPIE 3670 (1999) 144.
[19] Y.J. Rao, P.J. Henderson, D.A. Jackson, L. Zhang, I. Bennion, Electron. Lett. 33 (1997) 2063.
[20] T. Liu, G.F. Fernando, Z.Y. Zhang, K.T.V. Grattan, Sens. Actuators A: Phys. 80 (2000) 208.
[21] M. Singh, C.J. Tuck, G.F. Fernando, Smart Mater. Struct. 8 (1999) 549.
[22] T. Liu, G.F. Fernando, Y.J. Rao, D.A. Jackson, L. Zhang, I. Bennion, Proc. SPIE 3042 (1997) 203.
[23] H.K. Kang, D.H. Kang, C.S. Hong, C.G. Kim, Smart Mater. Struct. 12 (2003) 29.
[24] L.A. Ferreira, A.B. Lobo Ribeiro, J.L. Santos, F. Farahi, Smart Mater. Struct. 7 (1998) 189.
[25] V.R. Machavaram, R.A. Badcock, G.F. Fernando, Meas. Sci. Technol. 18 (2007) 928.
[26] V.R. Machavaram, R.A. Badcock, G.F. Fernando, Sens. Actuators A: Phys. 138 (2007) 248.
[27] Y.J. Rao, Z.L. Ran, X. Liao, H.Y. Deng, Opt. Exp. 15 (2007) 14936.
[28] L. Li, X.L. Tong, C.M. Zhou, H.Q. Wen, D.J. Lv, K. Ling, C.S. Wen, Opt. Commun. 284 (2011) 1612.
[29] X.D. Jin, J.S. Sirkis, J.K. Chung, V.S. Venkat, J. Intell. Mater. Syst. Struct. 9 (1998) 171.
[30] R.A. Badcock, G.F. Fernando, Proc. SPIE 2444 (1995) 422.
[31] G.R. Powell, P.A. Crosby, G.F. Fernando, R.C. Spooncer, C.M. France, D.M. Waters, J. Smart. Mater. Struct. 7 (1998) 557.
[32] A. Martin, R. Badcock, C. Nightingale, G.F. Fernando, IEEE Photon. Technol. Lett. 9 (1997) 982.
[33] J.A. Etches, G.F. Fernando, Polym. Compos. 30 (2009) 1265.
[34] SC7640 auto/manual high resolution sputter coater operating manual, Quorum Technologies, Document number OM-SC7640, 01/02, 16-26.
[35] B. Degamber, D. Winter, J. Tetlow, M. Teagle, G.F. Fernando, Meas. Sci. Technol. 15 (2004) L5.
[36] B. Degamber, G.F. Fernando, J. Appl. Polym. Sci. 89 (2003) 3868.
[37] K.E. Chisholm, K. Sugden, I. Bennion, J. Phys. D: Appl. Phys. 31 (1998) 61.
[38] S. Pal, J. Mandal, T. Sun, K.T.V. Grattan, Appl. Opt. 42 (2003) 2188.
[39] A.D. Kersey, M.A. Davis, H.J. Patrick, M. LeBlanc, K.P. Koo, C.G. Askins, M.A. Putnam, E.J. Friebele, J. Lightwave Technol. 15 (1997) 1442.
[40] M. Ghorbanpour, C. Falamakiz, J. Nanostruct. Chem. 3 (2013) 1.
[41] A. Proszynski, D. Chocyk, G. Gladyszewski, Opt. Appl. 39 (2009) 705.
[42] V. Svorcik, O. Kvitek, O. Lyutakov, J. Siegel, Z. Kolska, Appl. Phys. A 102 (2011) 747.
[43] S.A. Kovalenko, Semicond. Phys. Quant. Electron. Optoelectron. 3 (2000) 514.
[44] V. Svorcik, J. Siegel, P. Sutta, J. Mistrik, P. Janicek, P. Worsch, Z. Kolska, Appl. Phys. A 102 (2011) 605.
[45] S. Pal, T. Sun, K.T.V. Grattan, S.A. Wade, S.F. Collins, G.W. Baxter, B. Dussardier, G. Monnom, Sens. Actuators A 112 (2004) 211.
[46] H.J. Yoon, D.M. Costantini, H.G. Limberger, R.P. Salathe, C.G. Kim, V. Michaud, J. Intell. Mater. Syst. Struct. 17 (2006) 1059.
[47] V.R. Machavaram, L. Wang, S.D. Pandita, S. Hellmann, F.N. Bogonez, G.F. Fernando, J. Appl. Polym. Sci. (2014) 41088, http://dx.doi.org/10.1002/AP.P.41088.

Biographies

Abilash Nair obtained his Bachelor of Technology in Polymer Engineering from Mahatma Gandhi University, Kerala, India in 2003. From 2003 to 2006, he worked with CEAT Ltd, Mumbai, one of the leading tyre manufacturers in India and gained experience in the tyre industry. In 2006, he undertook an MSc in Polymer Science and Engineering from London Metropolitan University, UK. In 2008, he was awarded an Overseas Research Studentship to pursue his PhD at the University of Birmingham, UK. His PhD research was on the process and structural health monitoring of advanced fibre reinforced composites using optical fibre sensors. He is currently working as a materials development engineer at Dunlop Aircraft tyres Ltd, Birmingham. His research interests are in multi-measurand optical fibre sensors for process monitoring and rubber compound development for the manufacture of aircraft tyres. He is a professional graduate member of the Institute of Materials, Minerals and Mining and an active member of the Rubber in Engineering Group.

Venkata R. Machavaram obtained his Bachelor's and Master's degrees from Andhra Loyola College and University of Hyderabad, India respectively. He was awarded PhD in 2006 for his work on the development of micromachining techniques for the production of fibre Fabry–Perot sensors by Cranfield University, UK. He worked on the development of novel low-cost fibre sensors for process and structural integrity monitoring of aerospace composites; and energy efficient manufacturing techniques for composites during his postdoctoral research in Sensors & Composites Group, University of Birmingham, UK. He is currently a faculty member at the School of Electronics Engineering, VIT University, Tamil Nadu, India. His current research activities include development of smart fibre sensors for automotive and biomedical applications.

Ramani S. Mahendran is an Applications Development Scientist at Malvern Instruments Ltd, Wocestershire, UK. She received her BSc from University of Moratuwa, Sri Lanka and her PhD from School of Metallurgy and Materials, University of Birmingham, UK before being employed as a Research Associate in Sensors and Composites Group, School of Metallurgy and Materials, University of Birmingham. Ramani has designed and demonstrated the use of fibre optic sensors for cure monitoring and the detection of moisture ingress in thermosetting resins.

Christophe Paget received his Master of Engineering (Hons) in Mechatronics from the University of Valenciennes, France. He received his PhD in Electronics from the University of Valenciennes in early 2001 and his PhD in Aeronautics from the Royal Institute of Technology of Stockholm late 2001. He worked for the Swedish Defence Research Agency (FOI), Stockholm, Sweden from 1996 till 2002 on structural health monitoring. He now works at the Materials and Processes Department of Airbus in the UK, since March 2002, leading the A350 Materials & Processing Integration team, where he carried out his work on SHM to date. He received his honorary visiting Professorship from University of Cardiff, UK in 2011 for his contribution to SHM.

Colin Barrow graduated from the University of York with a BSc (Hons) Degree in Chemistry in the early nineties. After laboratory based positions at National Power and British Gypsum, in 1998 Colin moved to a Technical Sales role at Bruker UK Ltd within the Bruker Optics product group, which is responsible for promotion of Vibrational Spectroscopy products (FTIR, NIR and Raman Instrumentation). Over the next 16 years Colin has gained a wealth of experience supplying FTIR, NIR and Raman spectrometers to Industry and Academia, supporting a wide range of applications. Industrial markets covered include Food, Polymer, Petrochemical, Chemical and Pharmaceutical industries. Spectrometer applications range from laboratory based systems for quality control; to high performance spectrometers for R&D; to fibre optic, probe based systems for in-line process monitoring and real time analysis. In 2008 Colin was promoted to the role of Country Manager, Bruker Optics and he continues to work closely with a team of sales specialists and application scientists to implement applications of FTIR, NIR and Raman spectrometers in many areas of Academia and Industry.

Gerard F. Fernando holds the Chair of Polymer Engineering at the University of Birmingham, School of Metallurgy and Materials. After securing his PhD (Fatigue of hybrid composites) from the School of Materials Science, University of Bath, UK, he work at the Water Research Centre, Swindon, UK where he was responsible for condition monitoring of buried plastic pipeline systems and welding of plastic pipes. He then moved to the Materials Technology Department, Brunel University as a lecturer in Polymer Chemistry. Professor Fernando's research interests are focused on the clean process of composites and the development of low-cost optical sensor systems for fibre reinforced composites.